International Journal of Medical Microbiology 309 (2019) 130–142

Contents lists available at ScienceDirect

International Journal of Medical Microbiology

journal homepage: www.elsevier.com/locate/ijmm

Alterations on growth and cell organization of *Giardia intestinalis* trophozoites after treatment with KH-TFMDI, a novel class III histone deacetylase inhibitor

Ana Paula R. Gadelha[a], Bárbara Bravim[a], Juliana Vidal[b], Lissa Catherine Reignault[b], Bruno Cosme[a], Kilian Huber[c,d], Franz Bracher[c], Wanderley de Souza[a,b,e,*]

[a] Diretoria de Metrologia Aplicada a Ciências da Vida, Instituto Nacional de Metrologia, Qualidade e Tecnologia, Rio de Janeiro, RJ, Brazil
[b] Instituto de Biofísica Carlos Chagas Filho, Universidade Federal do Rio de Janeiro, Rio de Janeiro, RJ, Brazil
[c] Department of Pharmacy, Center for Drug Research, Ludwig-Maximilians-University of Munich, Munich, Germany
[d] Nuffield Department of Medicine, University of Oxford, Oxford, UK
[e] Instituto Nacional de Ciência e Tecnologia em Biologia Estrutural e Bioimagens e Centro Nacional de Biologia Estrutural e Bioimagens, Universidade Federal do Rio de Janeiro, Rio de Janeiro, RJ, Brazil

ARTICLE INFO

Keywords:
Giardia intestinalis
Class III NAD+-dependent histone deacetylases inhibitor
Automated quantitative fluorescence microscopy
Electron microscopy
Proliferation
Cell death

ABSTRACT

Giardia trophozoites have developed resistance mechanisms to currently available compounds, leading to treatment failures. In this context, the development of new additional agents is mandatory. Sirtuins, which are class III NAD$^+$-dependent histone deacetylases, have been considered important targets for the development of new anti-parasitic drugs. Here, we evaluated the activity of KH-TFMDI, a novel 3-arylideneindolin-2-one-type sirtuin inhibitor, on *G. intestinalis* trophozoites. This compound decreased the trophozoite growth presenting an IC_{50} value lower than nicotinamide, a moderately active inhibitor of yeast and human sirtuins. Light and electron microscopy analysis showed the presence of multinucleated cell clusters suggesting that the cytokinesis could be compromised in treated trophozoites. Cell rounding, concomitantly with the folding of the ventro-lateral flange and flagella internalization, was also observed. These cells eventually died by a mechanism which lead to DNA/nuclear damage, formation of multi-lamellar bodies and annexin V binding on the parasite surface. Taken together, these data show that KH-TFMDI has significant effects against *G. intestinalis* trophozoites proliferation and structural organization and suggest that histone deacetylation pathway should be explored on this protozoon as target for chemotherapy.

1. Introduction

Giardia intestinalis is a flagellated protozoan and the causative agent of giardiasis, a disease characterized by symptoms such as chronic diarrhea, nausea and a stomach cramps (Buret, 2008). *Giardia* is a waterborne parasitic protozoan with a worldwide distribution (Karanis et al., 2007). Current giardiasis treatment is based on 5-nitroimidazole compounds, of which metronidazole is the most commonly used drug in many countries. This compound is activated in *G. intestinalis* when the 5-nitro group is reduced by oxidoreductase enzymes (Gardner and Hill, 2001; Emery et al., 2018) and the toxic metabolites formed by reduction can interact with several cell structures and molecular targets (Campanati and Monteiro-Leal, 2002; Oxberry et al., 1994; Uzlikova et al., 2014). Other compounds used to treat giardiasis are benzimidazole derivatives, such as albendazole, which bind to tubulin (MacDonald et al., 2004), inhibiting *Giardia* growth and changing cytoskeletal elements (Morgan et al., 1993; Pérez-Rangel et al., 2013). Metronidazole and albendazole were first developed to treat other parasitic infections, and introduced for giardiasis treatment about five decades ago. Although these drugs are still used against giardiasis, treatment failures and parasite resistance emerged over the decades (Argüello-García et al., 2009; Tejman-Yarden and Eckmann, 2011). Therefore, because of the prevalence of the disease, the development of new therapeutic agents is mandatory.

Histone acetylation is controlled by the activity of histone acetyltransferases (HATs), which contribute to chromatin decondensation and activation of transcription, and histone deacetylases (HDACs), which promote chromatin condensation and gene silencing

* Corresponding author at: Laboratório de Ultraestrutura Celular Hertha Meyer, Instituto de Biofísica Carlos Chagas Filho, Universidade Federal do Rio de Janeiro, Avenida Carlos Chagas Filho, 373, CCS, Bloco G-subsolo, Cidade Universitária, 21941-902 Rio de Janeiro, RJ, Brazil.
E-mail address: wsouza@biof.ufrj.br (W. de Souza).

https://doi.org/10.1016/j.ijmm.2019.01.002
Received 1 March 2018; Received in revised form 30 December 2018; Accepted 14 January 2019

(Kouzarides, 2007). In mammalian cells, HDACs are grouped into different classes, consisting of the ubiquitously expressed class I (HDACs 1–3, 8), the tissue-specific classes II (HDACs 4–7, 9, 10) and IV (HDAC11), and class III, composed of seven sirtuins (SIRT1-7). Sirtuins cleave the acetyl groups from lysine residues in histones and other proteins in a unique manner, since they are not zinc-dependent, but require nicotinamide adenine dinucleotide (NAD^+) as a co-factor for catalysis (Abend and Kehat, 2015). Sirtuins target different acetylated protein substrates and are localized to distinct cell compartments. They modulate numerous cellular processes, including the cell cycle, microtubule organization, mitochondrial activity, DNA repair, and cell death (Horio et al., 2011; Inoue et al., 2007; Verdin et al., 2010). Sirtuins have also been found in various parasitic protozoa, including *Plasmodium falciparum*, where they were associated with antigenic variation regulation (Merrick et al., 2015). In the trypanosomatid parasites *Trypanosoma cruzi* (Ritagliati et al., 2015) and *Trypanosoma brucei* (Alsford et al., 2007), sirtuin activity was important for the proliferation of replicative forms, the host cell-parasite interaction, cell differentiation, and DNA repair. Sirtuin expression was also detected in *Leishmania* (Vergnes et al., 2005; Zemzoumi et al., 1998), in which Sir2-related proteins were involved in the control of survival and cell death. The analysis of *G. intestinalis* genome showed the presence of five sirtuin type 2 family homologues: GL50803_10708, GL50803_10707, GL50803_11676, GL50803_6942 and GL50803_16569 (Sonda et al., 2010; Giardia DB: http://giardiadb.org). As pointed out by Carranza et al. (2016), three *Giardia* sirtuins (GL50803_10707; GL50803_10708; GL50803_11676) may be phylogenetically classified as belonging to class I, whereas other two sirtuins are more closely to class III Sirt5 from human (GL50803_16569) and subclass U of bacterial sirtuins (GL50803_6942) (Religa and Waters, 2012; Wang et al., 2016). *Giardia* sirtuins are localized in the trophozoite nucleus, with exception of GL50803_10708, which has cytoplasmic localization and may not be related to genetic regulation (Carranza et al., 2016).

In view of the biological role played by HDAC, classic inhibitors of class III histone deacetylases have been commercially available and have become interesting alternatives for the treatment of neoplastic and age-associated diseases and other pathologies (Carafa et al., 2012). Sirtinol, a commercially available SIRT2 inhibitor, was investigated for its activity against *Leishmania infantum* and inhibited amastigote multiplication and promoted cell death associated with DNA fragmentation (Vergnes et al., 2005). Nicotinamide, a moderately active inhibitor of yeast and human sirtuins, was able to inhibit *Plasmodium falciparum* and *Trypanosoma cruzi* proliferation (Prusty et al., 2008; Soares et al., 2012) and *Giardia* encystation process (Carranza et al., 2016). When used against *T. cruzi* and *L. amazonensis,* KH-TFMDI, a novel 3-arylideneindolin-2-one-type inhibitor of NAD + dependent histone deacetylases (Huber et al., 2010), caused growth arrest and induced programmed cell death (Veiga-Santos et al., 2014; Verçoza et al., 2017). In view of these observations we decided to investigate the activity of KH-TFMDI on *G. intestinalis* trophozoites. The human sirtuins have three active pocket sites, A, B and C; the last one is proposed to have a regulatory role (Avalos et al., 2005). KH-TFMDI has similar activity to cambinol and nicotinamide, at least it shares the specific protein binding site in the C subpocket of the sirtuin 2 protein sequence (Avalos et al., 2005; Huber et al., 2010). The NAD + binding site (C subpocket) is highly conserved from protozoan taxa to human, suggesting that KH-TFMDI may have similar activity on different organisms. In the present study, we report that KH-TFMDI inhibits the proliferation of the *G. intestinalis* trophozoites and compromises cytokinesis. This compound also induces several ultrastructure changes. Despite that, these cells eventually die by a process characterized by DNA/nuclear damage, formation of the multi-lamellar bodies and annexin V binding on the cell surface. These results indicate that KH-TFMDI has noteworthy effects against *G. intestinalis*, suggesting that class III NAD+-dependent histone deacetylases are potential targets for development of new drugs to treat giardiasis in the future.

2. Methods

2.1. Sirtuin inhibitor

The sirtuin inhibitor KH-TFMDI was synthesized by Huber and Bracher (Huber et al., 2010) at the Department of Pharmacy, Center for Drug Research, Ludwig-Maximilians-University in Munich, Germany. The structure of this compound can be seen in the Supplementary material 1. KH-TFMDI is a member of the 3-arylideneindolin-2-one family, which was previously synthesized to inhibit the human class III NAD+-dependent histone deacetylases I and II (Huber et al., 2010; Ong et al., 2017). Stock solutions of the compound (10 mM) were prepared in dimethyl sulfoxide (DMSO) (Merck, Darmstadt, Germany) and stored at −20 °C. Metronidazole (Sigma Chemical Company, St. Louis, USA), used as a positive control, was dissolved in sterile water. Nicotinamide (Merck, Darmstadt, Germany), an inhibitor of *Giardia*, yeast and human sirtuins, was dissolved in sterile water at stock concentration of 1 M.

2.2. Parasites

Cultures of *Giardia intestinalis* trophozoites from the WB isolate (ATCC 30957, USA) were grown in 16-ml screw-cap glass culture tubes containing modified TYI-S-33 medium (pH 7.2) enriched with 0.1% bovine bile and 10% fetal bovine serum at 37 °C, for 48 to 72 h, as described by Keister (1983).

2.3. Intestinal epithelial cell cultures

Monolayers of human colon epithelial cells (Caco-2 line, ATCC HTB-37, USA) were grown in high-glucose Dulbecco's modified Eagle's medium (DMEM) with 10% fetal bovine serum (FBS) in an atmosphere of 5% CO_2 at 37 °C.

2.4. G. intestinalis proliferation assays

Trophozoites (1×10^5 cells/ml) were inoculated in fresh TYI-S-33 medium in the presence of 1, 5, 10, or 25 μM of KH-TFMDI. The maximum concentration of DMSO was lower than or equal to 0.5%, a concentration that does not interfere with *Giardia* growth (Campanati et al., 2001). Metronidazole was used as positive control at the concentration of 1, 5, 10, or 25 μM. Parasites were also exposed to 1, 10, 20 and 50 mM of nicotinamide. Following growth at 24 and 48 h, untreated and DMSO- or treated parasites were placed on ice for 15 min, cells were diluted 1:10 on 4% formaldehyde and counted using a hemocytometer (Neubauer chamber). For all drugs, the concentration that caused a 50% reduction in the reproduction of trophozoites (IC_{50}) was calculated using a dose response curve (log inhibitor vs response) from Prism 6 software (https://www.graphpad.com). All experiments were performed at least four times.

2.5. Mammalian cell cytotoxicity assays

Caco-2 cells were trypsinized and 1×10^4 cells/ml were inoculated in 96-well tissue culture plates. After 24 h, KH-TFMDI, at concentrations of 50 or 100 μM, was added to the culture medium and the plates were incubated at 37 °C in 5% CO_2 for 48 h. The final concentration of DMSO was lower than or equal to 1%. Following incubation with these compounds, cells were incubated with Hoechst 33342 (Molecular Probes, USA; 5 μg/ml) to identify nuclei. For quantification of the proliferation, live cells were imaged using the IN Cell Analyzer 2000 automated cell imaging system (GE Healthcare, UK). The Hoechst signal was detected with excitation 350/50 nm and emission 455/50 nm filters. Ten image fields (20× objective, image area 0.150 mm^2/field) were acquired per well, each with an exposure time of 200 ms. The Multi Target Analysis module for IN Cell Analyzer 3.7.2 was used to define and quantify the objects of interest. Nuclear segmentation was

chosen to identify Caco-2 cells with a minimum nuclear area of 80 μm^2 and sensitivity level of 80.

2.6. Live cell imaging

For live cell imaging, a drop of cell suspension in culture medium was placed onto a slide and gently covered with a coverslip. Control and treated samples were examined with a Zeiss AxioImager light microscope using differential interference contrast (DIC) and a 100× objective under ambient conditions. Images were collected with an Axiocam MRc5 camera driven by AxiVision software. Images were processed using Adobe Photoshop software.

2.7. Field emission scanning electron microscopy (FESEM)

Control and treated cultures were fixed for 1 h in a solution containing 2.5% glutaraldehyde in 0.1 M cacodylate buffer (pH 7.2) and post-fixed for 1 h with 1% osmium tetroxide (OsO_4) in 0.1 M cacodylate buffer. Cells were dehydrated in an ethanol series, critical point dried in a Leica EM CPD 030 apparatus using CO_2, and ion-sputtered with a platinum layer. Samples were observed in a FEI Quanta FEG 450 field emission scanning electron microscope.

2.8. Immunofluorescence microscopy

Giardia trophozoites were chilled on ice for 15 min to detach the cells, which were collected by centrifugation (10 min, 1500*g*), washed twice with PBS, and then allowed to adhere to previously poly-L-lysine-coated coverslips. After 3 min, the cells were fixed with 1% formaldehyde in PHEM buffer for 1 h. Next, cells were permeabilized with 0.5% Triton X-100 in the same buffer for 10 min, followed by a 1-h blocking step (PBS containing 3% bovine serum albumin (BSA), pH 8.0). The cells were then incubated in the presence of the primary antibody TAT-1 kindly provided by Dr. K. Gull (Kohl et al., 1999). After primary antibody incubation, the samples were washed four times with PBS + BSA and incubated for 1 h with the secondary antibody goat anti-mouse IgG coupled to Alexa 546, diluted 1:400 (Molecular Probes, USA). Cells were washed 3 times and incubated with Hoechst stain (Molecular Probes, USA; 5 μg/ml) for 10 min. As a control, the primary antibody was omitted from some samples. Slides were mounted using n-propyl gallate to reduce photobleaching, and fluorescence images were obtained using a Leica TCS SP5 confocal microscope with corresponding beam splitter and barrier filters for imaging.

2.9. Automated quantitative fluorescence microscopy

The samples were assayed as described for the immunofluorescence assay. Briefly, slides were imaged in the IN Cell Analyzer 2000 automated cell imaging system (GE Healthcare, UK). The Hoechst signal was detected with excitation 350/50 nm and emission 455/50 nm filters; the TAT-1 signal was detected with excitation 543/22 nm and emission 605/64 nm filters. Fifty image fields (100× objective, image area 0.006 mm^2/field) were acquired per coverslip, each with an exposure time of 500 ms. The IN Cell Developer Toolbox 1.9.2 was used to define and quantify the objects of interest. Nuclear segmentation was chosen to identify trophozoites with a minimum nuclear area of 0.70 μm^2 and sensitivity level of 92. Typically, a *G. intestinalis* nucleus measured 1–2 μm^2. A post-segmentation processing step was incorporated to eliminate segmentation areas that were less than 8 μm^2 with kernel size 3. The analyzed parameters were: nuclear area, nuclear intensity, cell area and tubulin labeling intensity.

2.10. Western blot analysis

Trophozoites were harvested, washed twice and resuspended in PBS containing protease inhibitors cocktail (Sigma, USA). Then, the cells were lysed with ten cycles of freezing and thawing. The total cell lysates were mixed with a solution containing 62 mM Tris-HCl, 7% glycerol, 2.5% SDS, 5% β-mercaptoethanol, 0.01% bromophenol blue and boiled for 5 min. Protein concentration was determined by using a Bio-Rad protein assay (Bio-Rad, USA). The lysates at the protein concentration of 35 μg were loading on 7.5% SDS-PAGE. After electrophoresis, proteins were transferred to nitrocellulose membranes, blocked with 5% non-fat milk for 1 h at room temperature and incubated for 2 h with anti-α-tubulin TAT-1 and anti-acetylated tubulin 6-11B-1 (Sigma, USA) antibody at 1:10 dilution. Then, the membranes was washed three times and incubated for 1 h with peroxidase-conjugated goat anti-mouse secondary antibody (Promega, USA). Membranes were washed as previously described and visualized using chemiluminescent substrate.

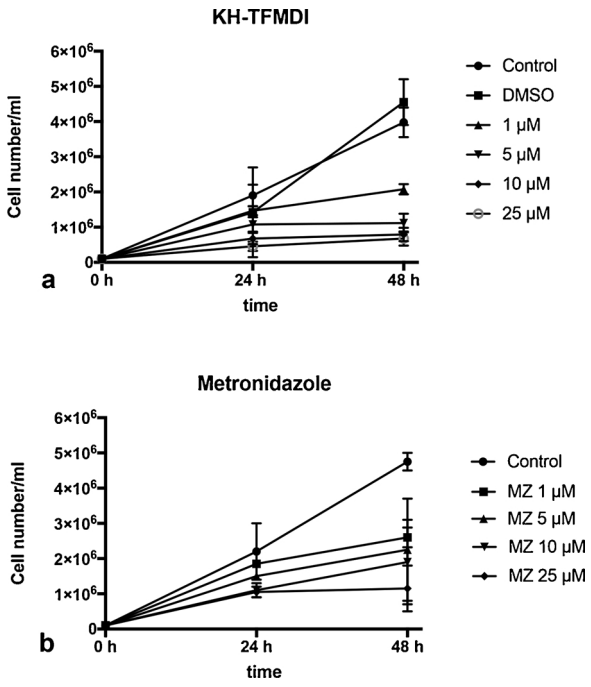

Fig. 1. Growth curves of treated trophozoites for 24 and 48 h. The parasite was cultured in the absence (control) or presence of the KH-TFMDI (a) and metronidazole (b) at the concentration of 1, 5, 10 and 25 μM. The number of parasites in each culture was determined using light microscopy and a hemocytometer, and the results are expressed as the mean ± SEM (n = 4).

2.11. Transmission electron microscopy (TEM)

For transmission electron microscopy, specimens were fixed for 1 h at room temperature in a solution containing 2.5% glutaraldehyde and 4% formaldehyde in PHEM buffer (pH 7.2). Samples were then washed twice in PBS, pH 7.2, and post-fixed in 1% OsO_4 supplemented with 0.8% potassium ferricyanide. Cells were then dehydrated in an acetone series, embedded in Epoxide resin and sectioned in a Reichert ultramicrotome. Ultrathin sections were collected in copper grids and stained with 5% aqueous uranyl acetate and lead citrate, and observed in a FEI Tecnai Spirit transmission electron microscope.

2.12. Annexin-V and propidium iodide analysis

This experiment was performed using a Dead Cell Apoptosis Kit with Annexin V-Alexa Fluor® 488 & Propidium Iodide (Molecular Probes, USA), following the manufacturer's protocol. Briefly, treated and untreated trophozoites were washed with chilled PBS and resuspended in 500 μl of 1× binding buffer. Cells were then incubated with Annexin V-Alexa 488 and propidium iodide for 5 min in the dark at room

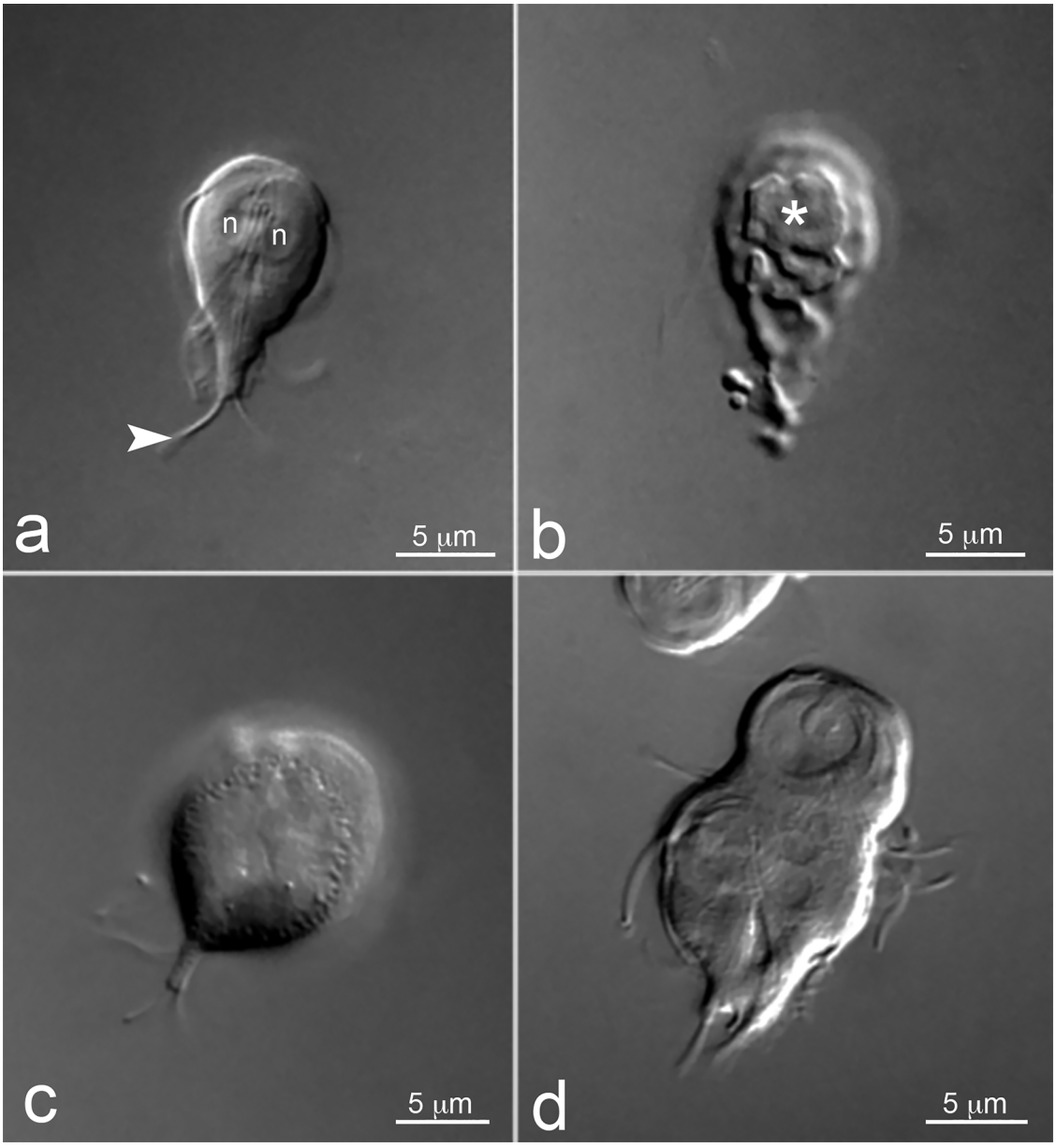

Fig. 2. Live cell images of *G. intestinalis* trophozoites in control and treated culture for 48 h. Untreated parasites exhibited normal morphology, with a pear shape, two nuclei (n) and flagella (arrowhead) (a). Cells treated with 1 μM of KH-TFMDI exhibited a ruffled aspect (*) of the surface (b). From treatment with 5 μM KH-TFMDI, cell rounding (c) and formation of asymmetric cell (d) were observed.

temperature. Data were collected on a BD FACSCalibur instrument controlled by CellQuest Pro software (BD Biosciences, CA, USA) and analyzed with Summit 4.3 (Dako, Fort Collins, CO, USA). A total of 10.000 events were acquired in the regions previously established as those corresponding to *G. intestinalis*. Alternatively, cells incubated with Annexin V-Alexa 488 and propidium iodide were analyzed by immunofluorescence using a Leica DMI600 B fluorescence microscope.

2.13. DNA fragmentation analysis

Total cellular DNA from treated and untreated cells was isolated and analyzed by acrylamide gel electrophoresis. Briefly, cells were mixed with a lysis buffer (100 mM Tris-HCl, 2 mM EDTA, 400 mM NaCl, 2% SDS, pH 8.0) containing 300 μg/ml of proteinase-K in a 56 °C water-bath for 90 min. Samples were centrifuged immediately at 7000 × *g* for 10 min at 4 °C and the supernatant was washed by adding 800 μl of 100% ethanol and centrifuged at 7000 × *g* for 10 min at 4 °C. After, the supernatant was decanted and the DNA pellet was washed by adding 800 μl of 100% ethanol and centrifuged at 7000 × *g* for 10 min at 4 °C. The resulting pellet was washed by adding 800 μl of 70% ethanol and centrifuged at 7000 × *g* for 12 min at 4 °C. The pellet was air-dried and resuspended in TE buffer, pH 7.5 (10 mM Tris–Cl, 0.1 mM of pH 8.0 EDTA). Total DNA was mixed with a tracking dye present in the sample buffer and loaded on a 7% acrylamide gel. Gels were run for 1 h at 165 V, stained with ethidium bromide, and analyzed using a UV transilluminator (Bio-Rad, USA).

2.14. Cell cycle analysis

Cells growth in 1.5 ml eppendorf tubes (approx. 10^5 cells in total) were chilled on ice for 20 min and collected by centrifugation (5 min; 1500*g*; 4 °C). Afterward, the medium was replaced, and the cells were fixed with ice cold 70% ethanol. The samples were then centrifuged, washed and resuspended in 500 μl of PBS containing 2.5 μl of RNase A

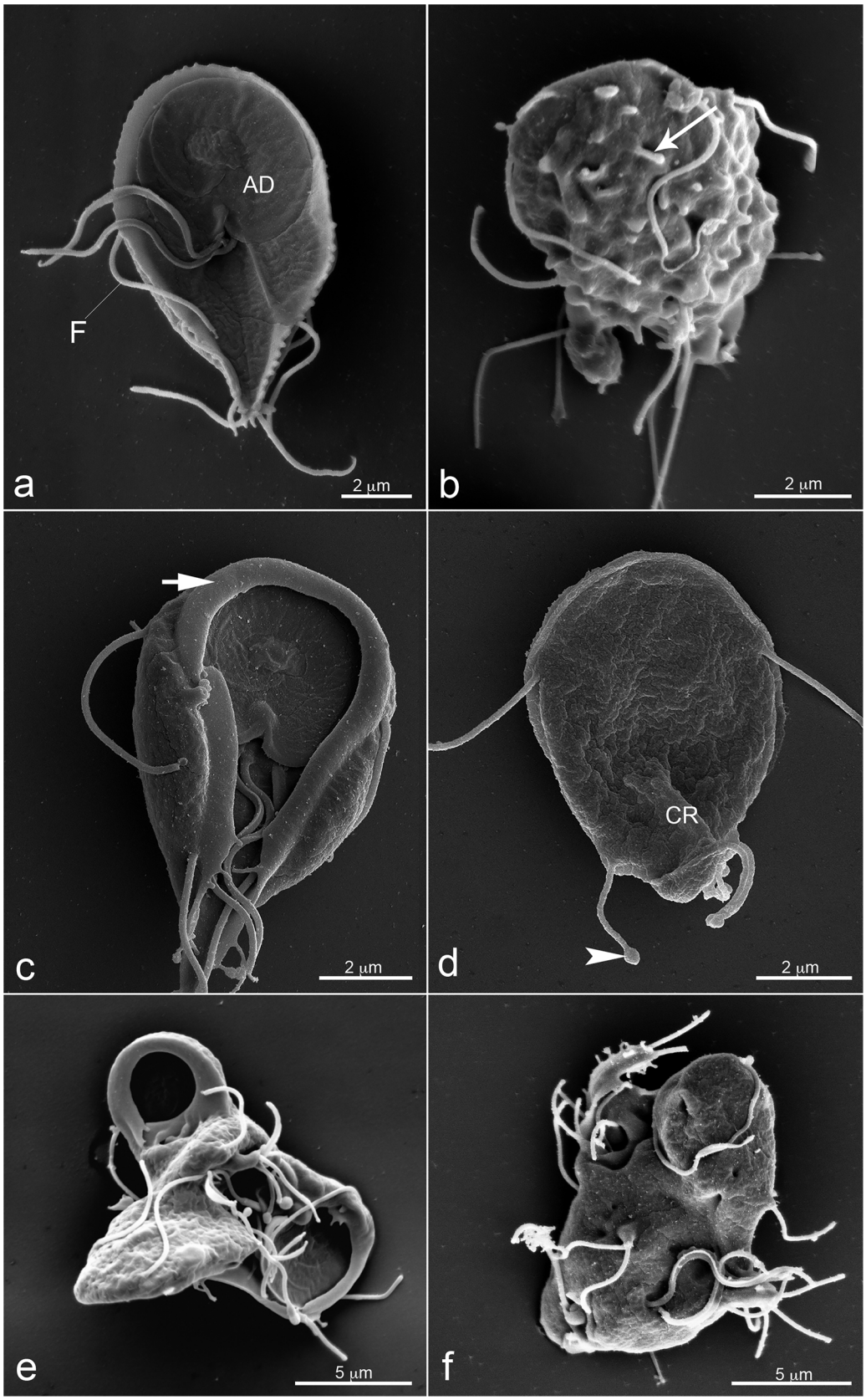

Fig. 3. Field emission scanning electron microscopy of *G. intestinalis* trophozoites. Untreated parasites exhibited normal morphology, with a pear shape, four anterior flagella (F), and an adhesive disk (AD) (a). Cells were treated with 1 μM KH-TFMDI for 48 h (b). Note the membrane blebbing (arrow) on the dorsal surface of the parasite. After treatment with 5 μM, the cell rounding associated with the ventro-lateral flange folding (small arrow) was observed (c). Note the shrinkage of the body's caudal portion (CR) and a large bulbous structure in the flagellar tip (arrowhead) of some parasites (d). Incomplete cell division and formation of cell masses (e–f) were observed after treatment.

corresponding to 50 μg/ml and incubated for 30 min at 37 °C. Then, the cells were centrifuged and resuspended in 500 μl of PBS containing propidium iodide at a final concentration of 2 μg/ml (Sigma, USA). The analysis was performed using an Accuri C6 cytometer (Becton Dickision, USA). Fifty thousand events were evaluated and the data plotted as cell percentage x cell cycle stage.

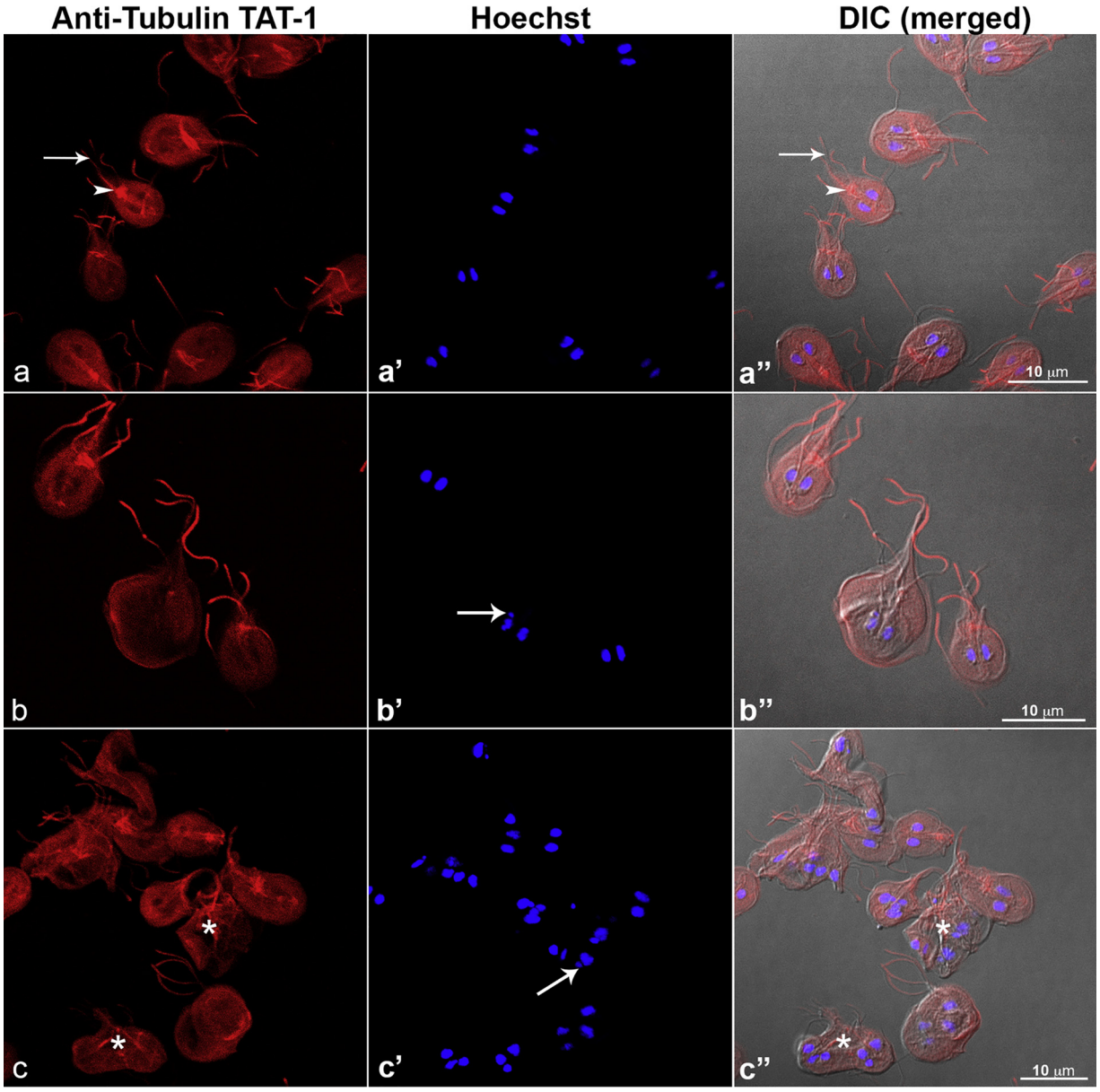

Fig. 4. Immunofluorescence microscopy using TAT-1 (a) and differential interference contrast (DIC) microscopy (a") of *G. intestinalis* trophozoites. Tubulin was concentrated in the flagella axonemes (arrow), median body (arrowhead), and the whole cell body of trophozoites (a, a"). Hoechst staining was used to label the two oval nuclei (a'). From treatment with 1 μM KH-TFMDI, some parasites showed a rounded aspect (b, b"). Different sizes of Hoechst-stained structures (arrow) were observed in treated cells (b"). Multinucleated cell masses (*) were seen after treatment with 5 μM KH-TFMDI (c, c"); an abnormal number of nucleus was also visualized (arrow).

2.15. Multiple sequence alignments

Different organisms protein sequences of sirtuins were acquire from NCBI (http://www.ncbi.nlm.nih.gov/): *Xenopus leavis* (NP_001088636), *Homo sapiens* SIRT1 (NP_036370.2) and SIRT2 (AAK51133.1), *Drosophila melanogaster* (AHN57421.1), *Giardia intestinalis* (EET01632), *Trypanosoma grayi* (KEG11227.1), *Leishmania infantum* (AF487351.1), *Entamoeba histolytica* (EHI5A_061340) and *Entamoeba invadens* (EIN_219010). The aminoacid multiple sequence alignments were performed with ClustalW v2.1 under BLOSUM62 score matrix to score pairs of aligned residues.

2.16. Statistical analysis

Values are expressed as mean ± standard error of the mean, and were compared by two-way ANOVA with a Bonferroni multiple comparison test or one-way ANOVA with Dunnet's multiple comparison test (Prism 6 Software Inc.), as appropriate. *P* values lower than 0.05 were considered statistically significant.

3. Results

3.1. Multiple sequence alignments

We performed a multiple sequence alignments of *Giardia* NAD-dependent histone deacetylase Sir2 (GL50803_10707) with the canonical fold of the sirtuins from several organisms (Supplementary material 2). These data showed a high level of similarity between *Giardia* NAD-dependent histone deacetylase Sir2 (GL50803_10707) and the orthologues of other protozoan and metazoan species (Supplementary material 2).

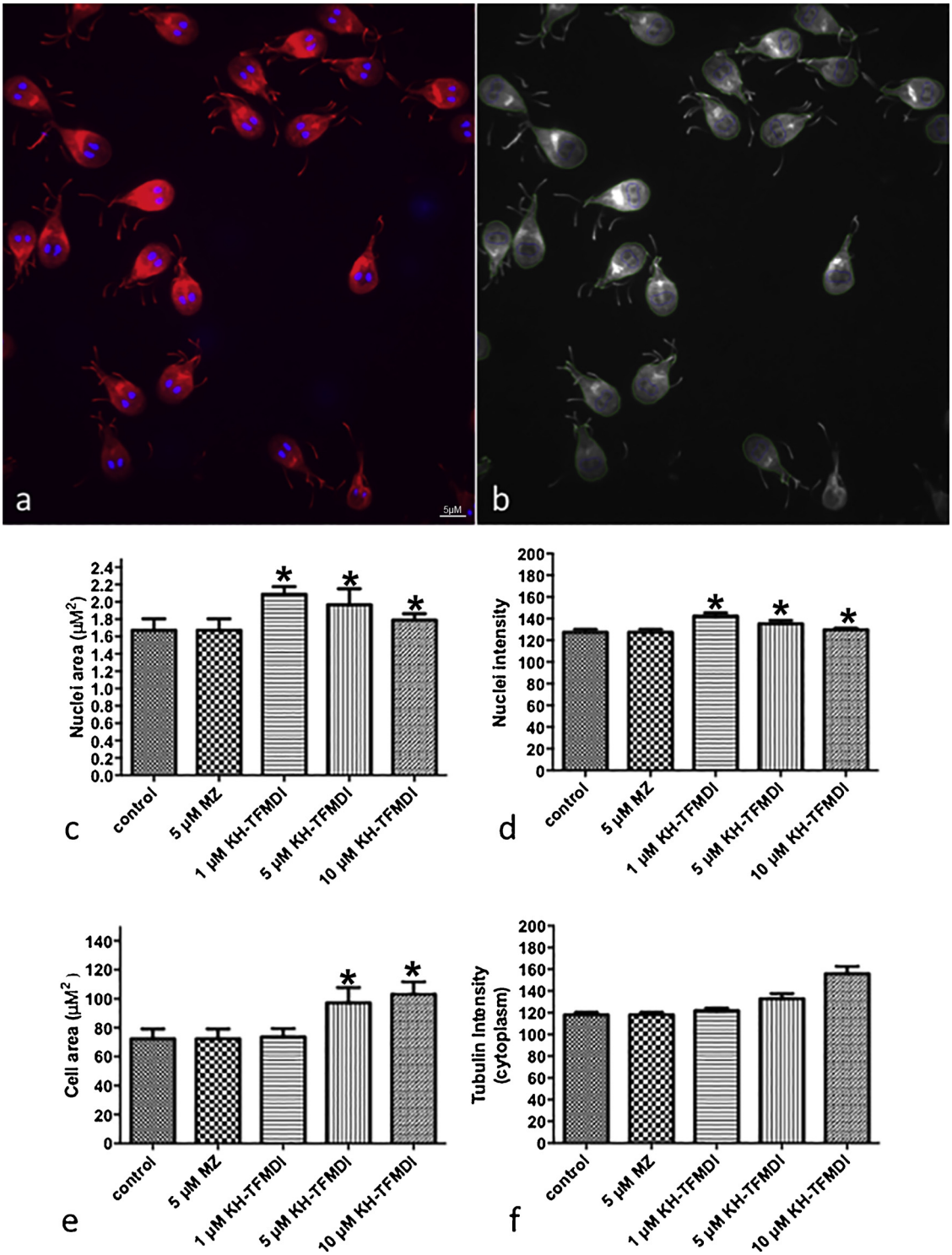

Fig. 5. Automated quantitative fluorescence microscopy of control and treated trophozoites. Example of images collected with the IN Cell imaging system (using a 100× objective) of control trophozoites. Cells were labeled with Hoechst–nucleus (blue) and anti-tubulin antibody TAT-1 (red) (a). The green line (b) indicates the segmentation of cell area by IN Cell Developer Toolbox 1.9.2. High content analysis of nuclei area (c), nuclei intensity (d), cell area (e) and cell (tubulin) intensity (f), was carried out during trophozoite treatment with different KH-TFMDI concentrations for 48 h. The values are expressed as the mean ± standard deviation (n = 500 cells) (For interpretation of the references to colour in this figure legend, the reader is referred to the web version of this article).

3.2. KH-TFMDI effects on parasite growth

In order to verify the activity of the sirtuin inhibitor KH-TFMDI on *G. intestinalis* proliferation, trophozoites were incubated with different concentrations of the compound for 24 and 48 h. The addition of KH-TFMDI led to dose- and time-dependent growth inhibition as shown in Fig. 1a. This compound significantly decreased the parasite replication ($p < 0.001$), presenting an IC_{50} value in the single digit μM range at 48 h of treatment. Incubation with 10 and 25 μM KH-TFMDI reduced around 80% cell growth. The concentration of DMSO equivalent to those used in treated cells (i.e., up to 0.5%) did not affect parasite proliferation (Fig. 1a). Metronidazole, the reference drug used as a

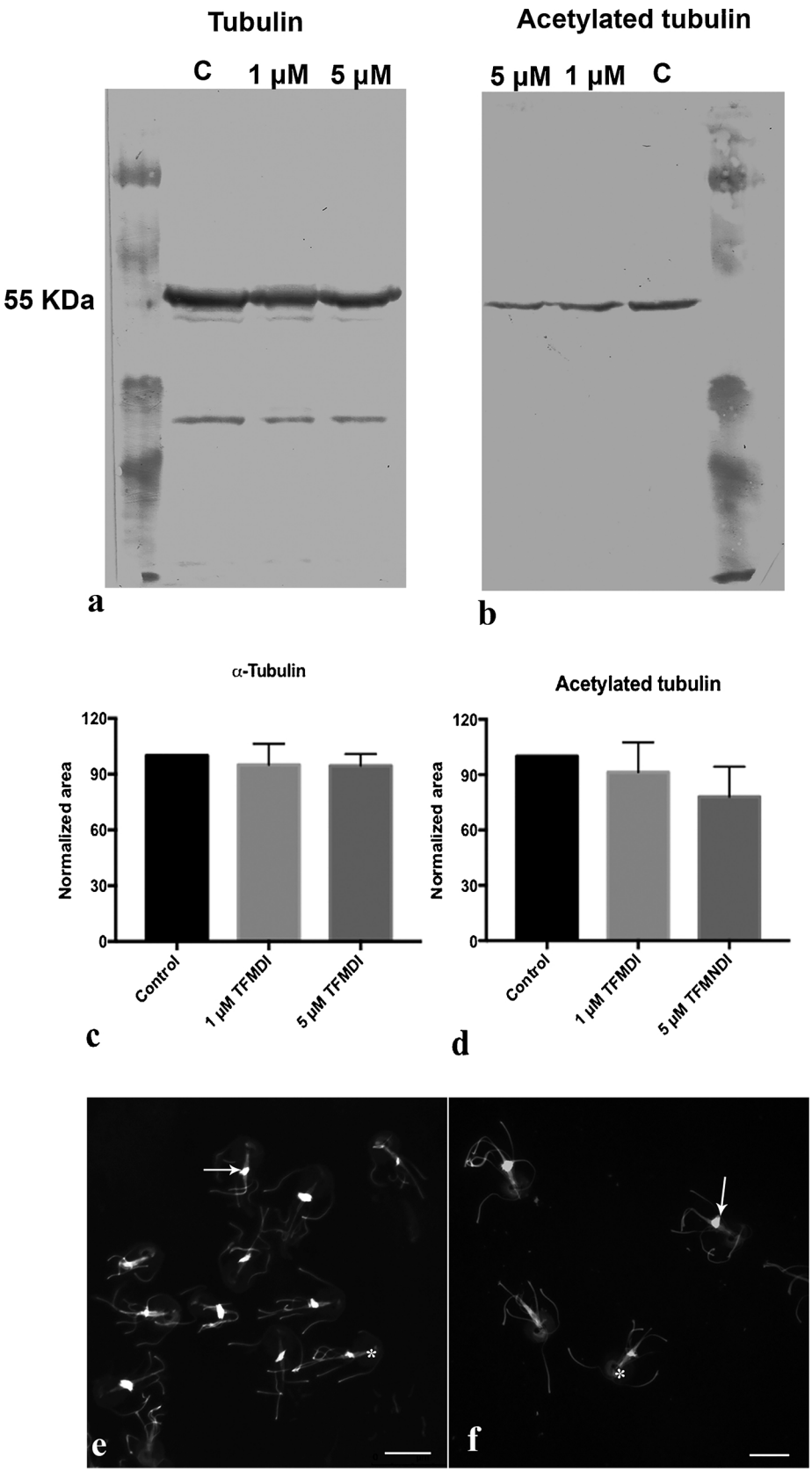

Fig. 6. Detection of α-tubulin and acetylated α-tubulin in control cells and trophozoites treated with KH-TFMDI by Western blot analysis and densitometry. Each lane was loaded with 35 µg of protein of whole cell lysates. Immunoblotting using anti-α-tubulin (a) and anti-acetylated α-tubulin antibodies (b). Densitometry analysis of the anti-α-tubulin (c) and anti-acetylated α-tubulin labeling (d). The values plotted in the graphics were normalized using the measurement of the area related to the labeling of the SDS-PAGE gel. The results indicate that there was a slight decreased in the amount of acetylated α-tubulin after treatment with 5 µM KH-TFMDI, however, this reduction was not significant (n = 3 independent experiments). Immunofluorescence microscopy showed that acetylated tubulin was concentrated in the flagella axonemes, median body (arrows) and adhesive disk (*) of the control (e) and treated trophozoites (f).

positive control, reduced parasite replication exhibiting an IC_{50} value in the single digit µM range (Fig. 1b). Nicotinamide was also tested and inhibited trophozoite growth presenting an IC_{50} value in the mM range (Supplementary material 3).

3.3. Cytotoxicity of KH-TFMDI on mammalian cell viability

During infection *Giardia* trophozoites attach and colonize the intestinal epithelium. To analyze the cytotoxicity effects on the

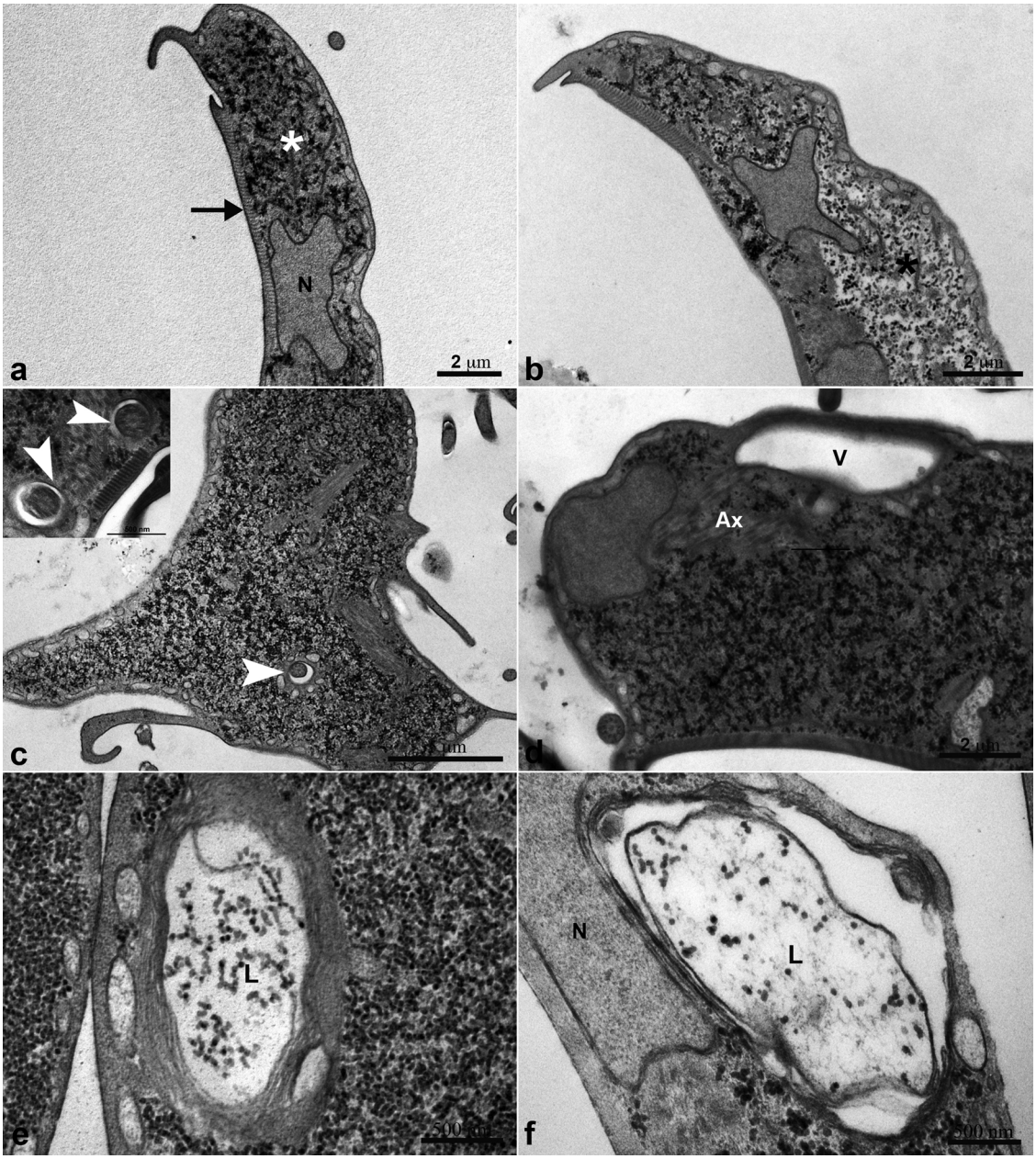

Fig. 7. Ultrathin sections of trophozoites observed by transmission electron microscopy. *G. intestinalis* (a) showing the nucleus (N), the adhesive disk (arrow), and the typical aspect of the cytoplasm (*) of control parasites (a). Cells treated with KH-TFMDI for 48 h (b–f). Note the abnormal distribution of the cytoplasmic contents (*) after treatment with 1 µM KH-TFMDI (b). After incubation with 5 µM KH-TFMDI changes in the cell shape was observed (c), some flagella were internalized in vacuoles (arrowheads in c and inset). Large vacuoles (L) were seen in the cytoplasm of treated cells (e–f).

mammalian host cells, Caco-2 intestinal cell line was treated for 48 h with 50 or 100 µM KH-TFMDI (i.e., 50- and 100-fold higher than the IC_{50} obtained for. *G. intestinalis* trophozoites). As shown in Supplementary material 4, KH-TFMDI or metronidazole did not alter the intestinal cells proliferation ($p > 0.05$).

3.4. KH-TFMDI effects on parasite morphology

As the concentration of 25 µM KH-TFMDI caused severe effects on cell growth, it was not included in the subsequent morphological and biochemical assays. Then, to investigate the primary effects of KH-TFMDI on cell structure, parasites were observed after exposure to lower concentrations. Live cell imaging observations showed that untreated cells presented the characteristic pyriform shape with the flagella and two nuclei (Fig. 2a). After exposure to 1 or 5 µM of KH-TFMDI, trophozoites presented a ruffled surface (Fig. 2b) and rounded appearance (Fig. 2c). Cell division was asymmetric after treatment with this inhibitor (Fig. 2d). Analysis by FESEM of fixed cells confirmed the morphological changes showed by light microscopy. When compared to control trophozoites (Fig. 3a), the parasites treated with 1 or 5 µM exhibited blebbing on their dorsal surface (Fig. 3b). Cell rounding was observed concomitantly with the folding of the ventro-lateral flange (Fig. 3c) in 31% of the population. KHTFMDI treatment altered flagella number of 22% of the parasites and a large bulbous structure in the flagellar tip could be observed (Fig. 3d). In addition, the formation of large cellular masses was also visualized (15% of cells) mainly after incubation with 10 µM (Fig. 3e–f).

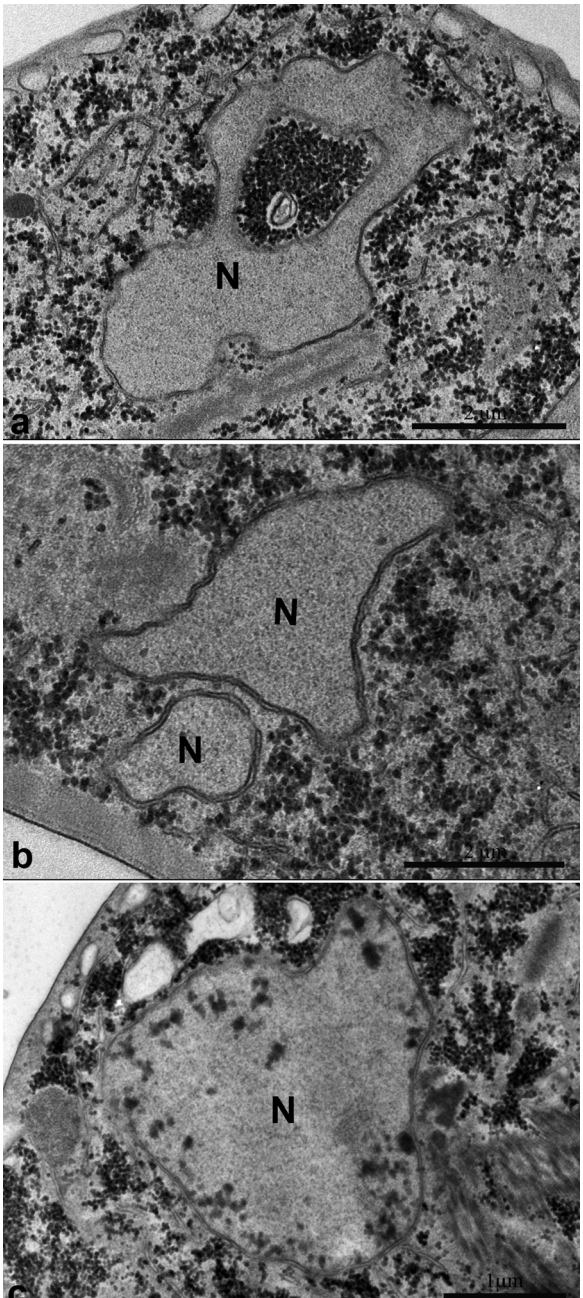

Fig. 8. Ultrathin sections of *G. intestinalis* treated with KH-TFMDI for 48 h. The nucleus (N) exhibited an abnormal shape profile (a–b) and condensed chromatin (c).

3.5. Nuclei and cytoskeleton organization after KH-TFMDI exposure

To better visualize the changes of the cell body and determine the distribution of the cytoskeletal elements, trophozoites were analyzed using DIC microscopy associated with immunofluorescence using the anti-α tubulin antibody TAT-1 and Hoechst stain to label the nuclei. In control cells, tubulin was observed in the flagella, median body, and cytoplasm (Fig. 4a, a"). The two nuclei of trophozoites were localized in the anterior region and presented an oval aspect (Fig. 4a'–a"). As observed in live cell imaging and FESEM assay, the pyriform shape of trophozoites slightly changed to a rounded aspect after treatment with 1 or 5 µM KH-TFMDI (Fig. 4b, b"). Different sizes of Hoechst-stained structures were observed in treated cells (Fig. 4b'). After exposure to KH-TFMDI cell cluster were seen with completed karyokinesis (Fig. 4c–c").

To quantify the morphological changes in the cell body and nucleus of the trophozoites exposed to KH-TFMDI, morphometric analysis were carried out using automated quantitative fluorescence microscopy. This methodology consists in the sequential acquisition of fluorescent images, identification and segmentation of the cell structures and data analysis (quantification, measurement) by automated algorithms included in IN Cell Investigator software. For this, the parasite nuclei and cell body segmentation were based on Hoechst nuclear staining and α-tubulin labeling, respectively (Fig. 5a–b). Morphometric analysis of parasite exposed to KH-TFMDI showed that the nuclear area and labeling intensity (Hoechst stain) increased 25% and 11% on treated parasites ($p < 0.05$) (Fig. 5c–d). Whereas the cell body area increased 45% when compared to control cells (Fig. 5e). This analysis also revealed that treated parasites increased up to 32% the α-tubulin labeling intensity (cell intensity) ($p < 0.05$) (Fig. 5f).

To investigate if KH-TFMDI could induce cytoskeleton changes associated to tubulin alterations, we carried out a Western blot analysis using anti-α-tubulin TAT-1 and anti-acetylated tubulin 6-11B-1 antibodies (Fig. 6a–b). The densitometry analysis indicated that there were no modifications in the amount of α-tubulin after treatment (Fig. 6c). The acetylated tubulin expression was slightly decreased within 48 h of addition of 5 µM KH-TFMDI, however this reduction was not significant (Fig. 6d). Immunofluorescence microscopy images and automated quantitative fluorescence microscopy showed that acetylated tubulin labeling pattern was similar in control and treated cells (Fig. 6e–f).

3.6. KH-TFMDI effects on parasite ultrastructure

Observations of longitudinal sections by TEM showed that untreated cells presented all the characteristic features of normal trophozoites: two round nuclei, intact adhesive disks, flagella axonemes, peripheral vesicles, and a homogeneous cytoplasm filled with ribosomes and glycogen particles (Fig. 7a). In contrast, incubation of the parasite with 1 to 10 µM KH-TFMDI led to an abnormal distribution of the cytoplasmic content, with areas lacking glycogen particles and ribosomes (Fig. 7b). Asymmetric cell shape profiles were also observed after exposure to the drug (Fig. 7c), as were cytoplasmic vacuolization and axoneme dislocation from characteristic locations (Fig. 7d). Although the structure of the cytoskeleton (adhesive disc, median body, flagella) has not been altered, some flagella were seen internalized (Fig. 7c). Multi-lamellar bodies, which contained cytoplasmic granules, were detected in the trophozoites (Fig. 7e–f). In some analysis, they were seen near dorsal surface and appeared to force the membrane, causing a protrusion (Fig. 7f). Ultrastructure changes were also observed in the nuclei that exhibited polymorphic aspects (Fig. 8a–b) and condensed chromatin (Fig. 8c) after incubation with KH-TFMDI.

3.7. Evaluation of annexin V binding on trophozoites

Flow cytometry analyses were carried out to determine if KH-TFMDI could induce early membrane events indicative of cell death in *G. intestinalis* trophozoites. Cells incubated with 1 and 10 µM KHTFMDI for 48 h were incubated in the presence of annexin V (a marker for early apoptosis) and propidium iodide (PI) (a marker for membrane damage, possibly late apoptosis/necrosis). Our results revealed that the percentage of labeling with annexin V for control cells was 1% of trophozoites, while the number of PI-positive parasites was 9% (Fig. 9a). In cultures exposure to KH-TFMDI, the levels of annexin V staining were about 50%, whilst levels of PI staining were around 1% (Fig. 9b–c). The annexin V labeling on parasite exposure to KH-TFMDI was confirmed by immunofluorescence microscopy images (Supplementary material 5).

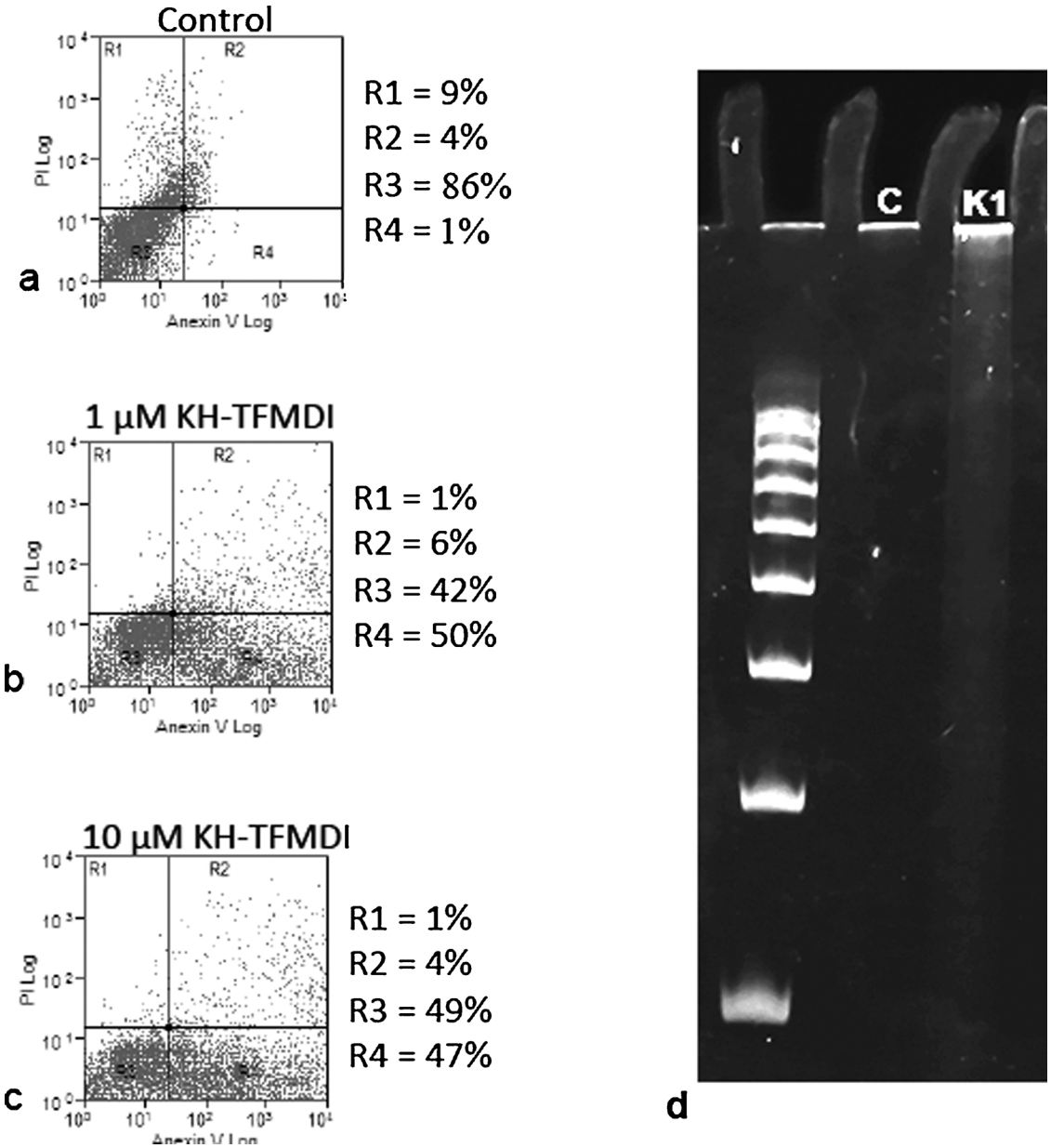

Fig. 9. Quantification of parasites by flow cytometry for 48 h. Non-treated parasites (a), cells treated with 1 and 10 µM KH-TFMDI, respectively (b–c). Left-upper quadrant (R1): positive only for PI; right-upper quadrant (R2): double-positive for annexin V and PI; left-bottom quadrant (R3): no labeling; right-bottom quadrant (R4): positive only for annexin V (b–c). Ten thousand gated events were harvested from each sample. Gel electrophoresis of DNA obtained from the control culture and trophozoites treated with 1 µM KH-TFMDI (d). Lane 1) 100bp ladder DNA marker; Lane 2) control cells (C); and Lane 3) KH-TFMDI (K1). Observe the sheared fragmented of the trophozoites DNA after treatment with 5 µM KH-TFMDI (n = 3 independent experiments).

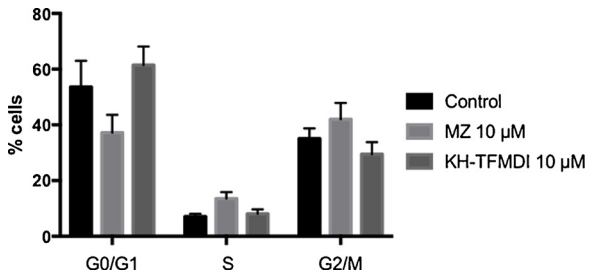

Fig. 10. Analysis of the cell cycle using propidium iodide by flow cytometry. *G. intestinalis* trophozoites were treated with 5 µM KH-TFMDI for 48 h. The results indicate that there was an increase in the population of cells in G0/G1 and S stage after exposure to KH-TFMDI. The image is representative of 3 independent experiments.

3.8. Analysis of DNA damage induced by KH-TFMDI treatment

The effect of the KH-TFMDI on *Giardia* DNA was also examined. When genomic DNA was isolated from trophozoites, sheared fragmented DNA mainly in lower molecular weight regions was detected in cells incubated with KH-TFMDI (Fig. 9d).

3.9. Cell cycle analysis

To determine the effects of KH-TFMDI on parasite division, cell cycle progression was followed by analysis of DNA content in control and treated cells by flow cytometer. It was observed a slightly increased (about 10%) in the percentage of cells in G0/G1 and S phase within 48 h of addition of 5 µM KH-TFMDI (Fig. 10).

4. Discussion

Our observations indicated that KH-TFMDI, a novel inhibitor of NAD + dependent histone deacetylases, significantly reduced the trophozoites proliferation. The *G. intestinalis* growth inhibition was similar to that found for *T. cruzi* (Veiga-Santos et al., 2014) and *L. amazonensis* (Verçoza et al., 2017) after exposure to this compound. The proliferation of *G. intestinalis* trophozoites was moderately reduced after exposure to nicotinamide. This reduction was similar that found in *Plasmodium*, *Leishmania* and *Trypanosoma* species which have characteristic Sir2 (Prusty et al., 2008; Sereno et al., 2005; Soares et al., 2012). Recently, Wang et al. (2016) showed that nicotinamide was able to inhibit activity of GL50803_10707 *Giardia* sirtuin with IC_{50} value of 4.47 mM. As previously demonstrated, *Giardia* sirtuins showed strong homology with SIRT1, and were mostly localized in the nucleus (Carranza et al., 2016; Wang et al., 2016). Since KH-TFMDI has shown activity against SITR1 in mammalian cell (Huber et al., 2010), it is possible that this compound also inhibit *Giardia* sirtuins. Thus, the effectiveness of KH-TFMDI and nicotinamide in *G. intestinalis* trophozoites indicate that NAD + dependent histone deacetylases could be potential pharmacological targets for giardiasis chemotherapy. It is important to note that KH-TFMDI exposure did not cause cytotoxicity in the Caco-2 cell line. Previous data indicated that KH-TFMDI had promising mammalian cell tolerance indexes when compared to other drugs currently used in clinical therapy for Chagas disease (Veiga-Santos et al., 2014). In accordance with the previously discussed (Veiga-Santos et al., 2014; Verçoza et al., 2017), KH-TFMDI was more selective for the parasite than mammalian cells.

The data obtained by light and electron microscopy showed cell rounding upon treatment with KH-TFMDI. This morphological alteration may be accompanied by changes in cytoskeletal elements, since they are associated with cellular stability. It is known that Sir2 proteins have a role in the cytoskeleton dynamics (Hubbert et al., 2002). Recently, Motonishi et al. (2015) reported that SIRT1 would be associated to deacetylating cortactin maintaining actin cytoskeleton integrity in podocytes. SIRT2 protein family, together with HDAC6, has a role in the tubulin deacetylation process regulating the microtubule dynamics in mammalian cells (Hubbert et al., 2002). In *L. amazonensis*, the sirtuin inhibitor KH-TFMDI was able to promote a light hyperacetylation of the tubulin that could be related to remodeling of the subpelicullar microtubules (Verçoza et al., 2017). Besides that, no change in the tubulin/acetylated tubulin expression or cytoskeleton structures (adhesive disk, median body, *funis*, and axonemes) were observed in *G. intestinalis* trophozoites treated with KH-TFMDI. Interestingly, cell rounding was associated with ventro-lateral flange folding and flagella internalization in trophozoits exposed to this compound. These morphological characteristics are similar to those reported during the first hours of the trophozoite encystation process (Midlej et al., 2009). It is important to mention that in the present study cyst wall protein expression was not observed in the treated culture (Supplementary material 6). Recently, it was demonstrated that treatment of *Giardia* trophozoites with nicotinamide or FR235222, an inhibitor of histone deacetylase (HDAC), blocked cyst wall protein synthesis and hence inhibited encystment (Carranza et al., 2016; Sonda et al., 2010).

Concomitant to the effect described above, several changes in the parasite's ultrastructure and process of cell division were noted. The presence of multinucleated and multiflagellated cell masses was seen, suggesting that the cytokinesis could be compromised in trophozoites exposed to this compound. Typical morphological characteristics of cell death seen in other studies (Bagchi et al., 2012; Corrêa et al., 2009), such as membrane blebbing, vacuoles and multi-lamellar bodies were frequently observed. Although *Giardia* is an amitochondrial organism, it presents some autophagic-like and apoptosis-like characteristics (Bagchi et al., 2012; Corrêa et al., 2009). Interestingly, previous works described that inhibition of histone deacetylases or sirtuin function would induce apoptosis in different cellular models (Zhang and Zhong, 2014), including parasites such as *T. cruzi*, *L. infantum* and *L. amazonensis* (Veiga-Santos et al., 2014; Verçoza et al., 2017; Vergnes et al., 2005). To determine if KH-TFMDI would induce cell death in *G. intestinalis* trophozoites, several classical markers were employed in the present study. Annexin V binding was observed in treated trophozoites, indicating that KH-TFMDI treatment could lead to early membrane events in cell death. DNA smear instead of DNA fragmentation, characteristic of cell death, was seen in trophozoites after drug exposure. This pattern was observed in other studies of cell death characterization on protozoa, indicating a different mechanism of DNA fragmentation in lower eukaryotes (Chose et al., 2002; Corrêa et al., 2009; Ghosh et al., 2009). The nuclear staining of the treated cells was more intense, possibly associated with chromatin condensation. The polymorphic aspect of the nuclei was related to the different sizes of Hoechst-stained structures, possibly indicating an early pyknosis-like process. The previous studies indicated that the activation of apoptosis-like cell death in *G. intestinalis* is different from the classical mechanism, occurring by a pathway independent of caspases (Bagchi et al., 2012; Corrêa et al., 2009). As the entire apoptotic machinery is absent in protozoa, alternative forms of programmed cell death have been considered (Bruchhaus et al., 2007).

Taken together, these observations indicate that KH-TFMDI promotes a stress condition that could lead to cell death of trophozoites. Consequently, KH-TFMDI should be considered a promising compound for the treatment of giardiasis due to its effects on protozoan proliferation and ultrastructure, in addition to low toxicity in human cell lines. The present work confirms the histone deacetylation pathway as an important target for the development of new strategies for giardiasis treatment.

Funding

This work was supported by the "Conselho Nacional de Desenvolvimento Científico e Tecnológico" (CNPq), "Financiadora de Estudos e Projetos" (FINEP), and "Fundação Carlos Chagas Filho de Amparo à Pesquisa no Estado do Rio e Janeiro (FAPERJ)".

Acknowledgments

The authors thank Jorge Gomes and Mariana Ribeiro for technical support with DNA analysis. The English language was revised by American Manuscript Editors.

Appendix A. Supplementary data

Supplementary material related to this article can be found, in the online version, at doi:https://doi.org/10.1016/j.ijmm.2019.01.002.

References

Abend, A., Kehat, I., 2015. Histone deacetylases as therapeutic targets-from cancer to cardiac disease. Pharmacol. Ther. 147, 55–62.
Alsford, S., Kawahara, T., Isamah, C., Horn, D., 2007. A sirtuin in the African trypanosome is involved in both DNA repair and telomeric gene silencing but is not required for antigenic variation. Mol. Microbiol. 63, 724–736.
Argüello-García, R., Cruz-Soto, M., Romero-Montoya, L., Ortega-Pierres, G., 2009. *In vitro* resistance to nitroimidazoles and benzimidazoles in *Giardia duodenalis*: variability and variation in gene expression. Infect. Genet. Evol. 9, 1057–1064.
Avalos, J.L., Bever, K.M., Wolberger, C., 2005. Mechanism of sirtuin inhibition by nicotinamide: altering the NAD(+) cosubstrate specificity of a Sir2 enzyme. Mol. Cell 17, 855–868.
Bagchi, S., Oniku, A.E., Topping, K., Mamhound, Z.N., Paget, T.A., 2012. Programmed cell death in *Giardia*. Parasitology 39, 894–903.
Bruchhaus, I., Roeder, T., Rennenberg, A., Heussler, V.T., 2007. Protozoan parasites: programmed cell death as a mechanism of parasitism. Trends Parasitol. 23, 376–383.
Buret, A.G., 2008. Pathophysiology of enteric infections with *Giardia duodenalis*. Parasite 15, 261–265.
Campanati, L., Monteiro-Leal, L.H., 2002. The effects of the antiprotosoal drugs metronidazole and furazolidone in trophozoits of *Giardia lamblia* (P1 strain). Parasitol. Res. 88, 80–85.

Campanati, L., Gadelha, A.P., Monteiro-Leal, L.H., 2001. Electron and video-light microscopy analysis of the in vitro effects of pyrantel pamoate on *Giardia lamblia*. Exp. Parasitol. 97, 9–14.
Carafa, V., Nebbioso, A., Altucci, L., 2012. Sirtuins and disease: the road ahead. Front. Pharmacol. 31, 3–4.
Carranza, P.G., Gargantini, P.R., Prucca, C.G., Torri, A., Saura, A., Svärd, S., Lujan, H.D., 2016. Specific histone modifications play critical roles in the control of encystation and antigenic variation in the early-branching eukaryote *Giardia lamblia*. Int. J. Biochem. Cell Biol. 81, 32–43.
Chose, O., Noel, C., Gerbod, D., Brenner, C., Viscogliosi, E., Roseto, A., 2002. A form of cell death with some features resembling apoptosis in the amitochondrial unicellular organism *Trichomonas vaginalis*. Exp. Cell Res. 276, 32–39.
Corrêa, G., Vilela, R., Menna-Barreto, R.F., Midlej, V., Benchimol, M., 2009. Cell death induction in *Giardia lamblia*: effect of beta-lapachone and starvation. Parasitol. Int. 58, 424–437.
Emery, S.J., Baker, L., Ansell, B.R.E., Mirzaei, M., Haynes, P.A., McConville, M.J., Svärd, S.G., Jex, A.R., 2018. Differential protein expression and post-translational modifications in metronidazole-resistant *Giardia duodenalis*. Gigascience 7. https://doi.org/10.1093/gigascience/giy024.
Gardner, T.B., Hill, D.R., 2001. Treatment of giardiasis. Clin. Microbiol. Rev. 14, 114–128.
Ghosh, E., Ghosh, A., Ghosh, A.N., Nozaki, T., Ganguly, S., 2009. Oxidative stress-induced cell cycle blockage and a protease-independent programmed cell death in microaerophilic *Giardia lamblia*. Drug Des. Dev. Ther. 3, 103–110.
Horio, Y., Hayashi, T., Kuno, A., Kunimoto, R., 2011. Cellular and molecular effects of sirtuins in health and disease. Clin. Sci. (Lond.) 121, 191–203.
Hubbert, C., Guardiola, A.C., Shao, R., Kawaguchi, Y., Ito, A., Nixon, A., Yoshida, M., Wang, X.F., Yao, T.P., 2002. HDAC6 is a microtubule-associated deacetylase. Nature 417, 455–458.
Huber, K., Schemies, J., Uciechowska, U., Wagner, J.M., Rumpf, T., Lewrick, F., Süss, R., Sippl, W., Jung, M., Bracher, F., 2010. Novel 3-arylideneindolin-2-ones as inhibitors of NAD+-dependent histone deacetylases (sirtuins). J. Med. Chem. 53, 1383–1386.
Inoue, T., Hiratsuka, M., Osaki, M., Oshimura, M., 2007. The molecular biology of mammalian SIRT proteins: SIRT2 in cell cycle regulation. Cell Cycle 6, 1011–1018.
Karanis, P., Kourenti, C., Smith, H., 2007. Waterborne transmission of protozoan parasites: a worldwide review of outbreaks and lessons learnt. J. Water Health 5, 1–38.
Keister, D.B., 1983. Axenic cultivation of *Giardia lamblia* in TYI-S-33 medium supplemented with bile. Trans. R. Soc. Trop. Med. Hyg. 77, 487–488.
Kohl, L., Sherwin, T., Gull, K., 1999. Assembly of the paraflagellar rod and the flagellum attachment zone complex during the *Trypanosoma brucei* cell cycle. J. Eukaryot. Microbiol. 46, 105–109.
Kouzarides, T., 2007. Chromatin modifications and their function. Cell 128, 693–705.
MacDonald, L.M., Armson, A., Thompson, A.R., Reynoldson, J.A., 2004. Characterisation of benzimidazole binding with recombinant tubulin from *Giardia duodenalis*, *Encephalitozoon intestinalis*, and *Cryptosporidium parvum*. Mol. Bioch. Parasitol. 138, 89–96.
Merrick, C.J., Jiang, R.H., Skillman, K.M., Samarakoon, U., Moore, R.M., Dzikowski, R., Ferdig, M.T., Duraisingh, M.T., 2015. Functional analysis of sirtuin genes in multiple *Plasmodium falciparum* strains. PLoS One 10. https://doi.org/10.1371/journal.pone.0118865.
Midlej, V., Benchimol, M., 2009. *Giardia lamblia* behavior during encystment: how morphological changes in shape occur. Parasitol. Int. 58, 72–80.
Morgan, U.M., Reynoldson, J.A., Thompson, R.C., 1993. Activities of several benzimidazoles and tubulin inhibitors against *Giardia* spp. *in vitro*. Antimicrob. Agents Chemother. 37, 328–331.
Motonishi, S., Nangaku, M., Wada, T., Ishimoto, Y., Ohse, T., Matsusaka, T., Kubota, N., Shimizu, A., Kadowaki, T., Tobe, K., Inagi, R., 2015. Sirtuin1 maintains actin cytoskeleton by deacetylation of cortactin in injured podocytes. J. Am. Soc. Nephrol. 26 1939–1359.
Ong, D.N., Dittrich, S., Swyter, S., Jung, M., Bracher, F., 2017. Synthesis of highly substituted 3-arylideneindolin-2-ones. Tetrahedron 73, 5668–5679.
Oxberry, M.E., Thompsonm, R.C.A., Reynoldson, J.A., 1994. Evaluation of the effects of albendazole and metronidazole on the ultrastructure of *Giardia duodenalis*, *Trichomonas vaginalis* and *Spironucleus muris* using transmission electron microscopy. Int. J. Parasitol. 24, 695–703.
Pérez-Rangel, A., Hernández, J.M., Castillo-Romero, A., Yépez-Mulia, L., Castillo, R., Hernández-Luis, F., Nogueda-Torres, B., Luna-Arias, J.P., Radilla, G., León-Avila, G., 2013. Albendazole and its derivative JVG9 induce encystation on *Giardia intestinalis* trophozoites. Parasitol. Res. 112, 3251–3257.
Prusty, D., Mehra, P., Srivastava, S., Shivange, A.V., Gupta, A., Roy, N., Dhar, S.K., 2008. Nicotinamide inhibits *Plasmodium falciparum* Sir2 activity in vitro and parasite growth. FEMS Microbiol. Lett. 282, 266–272.
Religa, A.A., Waters, A.P., 2012. Sirtuins of parasitic protozoa: in search of function(s). Mol. Biochem. Parasitol. 185, 71–88.
Ritagliati, C., Alonso, V.L., Manarin, R., Cribb, P., Serra, E.C., 2015. Overexpression of cytoplasmic TcSIR2RP1 and mitochondrial TcSIR2RP3 impacts on *Trypanosoma cruzi* growth and cell invasion. PLoS Negl. Trop. Dis. 9 (4), e0003725.
Sereno, D., Alegre, A.M., Silvestre, R., Vergnes, B., Ouaissi, A., 2005. *In vitro* antileishmanial activity of nicotinamide. Antimicrob. Agents Chemother. 49, 808–812.
Soares, M.B., Silva, C.V., Bastos, T.M., Guimarães, E.T., Figueira, C.P., Smirlis, D., Azevedo, W.F.Jr., 2012. Anti-*Trypanosoma cruzi* activity of nicotinamide. Acta Trop. 122, 224–229.
Sonda, S., Morf, L., Bottova, I., Baetschmann, H., Rehrauer, H., Caflisch, A., Hakimi, M.A., Hehl, A.B., 2010. Epigenetic mechanisms regulate stage differentiation in the minimized protozoan *Giardia lamblia*. Mol. Microbiol. 76, 48–67.
Tejman-Yarden, N., Eckmann, L., 2011. New approaches to the treatment of giardiasis. Curr. Opin. Infect. Dis. 24, 451–456.
Uzlikova, M., Nohynkova, E., 2014. The effect of metronidazole on the cell cycle and DNA in metronidazole-susceptible and -resistant *Giardia* cell lines. Mol. Biochem. Parasitol. 198, 75–81.
Veiga-Santos, P., Reignault, L.C., Huber, K., Bracher, F., De Souza, W., De Carvalho, T.M., 2014. Inhibition of NAD+-dependent histone deacetylases (sirtuins) causes growth arrest and activates both apoptosis and autophagy in the pathogenic protozoan *Trypanosoma cruzi*. Parasitology 141, 814–825.
Verçoza, B.R.F., Godinho, J.L.P., de Macedo-Silva, S.T., Huber, K., Bracher, F., de Souza, W., Rodrigues, J.C.F., 2017. KH-TFMDI, a novel sirtuin inhibitor, alters the cytoskeleton and mitochondrial metabolism promoting cell death in *Leishmania amazonensis*. Apoptosis 22, 1169–1188.
Verdin, E., Hirschey, M.D., Finley, L.W., Haigis, M.C., 2010. Sirtuin regulation of mitochondria: energy production, apoptosis, and signaling. Trends Biochem. Sci. 35, 669–675.
Vergnes, B., Sereno, D., Tavares, J., Cordeiro-da-Silva, A., Vanhille, L., Madjidian-Sereno, N., Depoix, D., Monte-Alegre, A., Ouaissi, A., 2005. Targeted disruption of cytosolic SIR2 deacetylase discloses its essential role in *Leishmania* survival and proliferation. Gene 363, 85–96.
Wang, Y.H., Zheng, G.X., Li, Y.J., 2016. *Giardia duodenalis* GlSir2.2, homolog of SIRT1, is a nuclear-located and AD+-dependent deacethylase. Exp. Parasitol. 169, 28–33.
Zemzoumi, K., Sereno, D., François, C., Guilvard, E., Lemesre, J.L., Ouaissi, A., 1998. *Leishmania major*: cell type dependent distribution of a 43 kDa antigen related to silent information regulatory-2 protein family. Biol. Cell 90, 239–245.
Zhang, J., Zhong, Q., 2014. Histone deacetylase inhibitors and cell death. Cell. Mol. Life Sci. 71, 3885–3890.